Research Article Vol. 30, No. 5 / 28 Feb 2022 / Optics Express 8248
Optics EXPRESS

Low-noise-figure and high-purity 10 vortex modes amplifier based on configurable pump modes

YAN WU,[1] JIANXIANG WEN,[1,*] MENGDI ZHANG,[1] JING WEN,[1] WEI CHEN,[1] XIAOBEI ZHANG,[1] FUFEI PANG,[1] FENGZAI TANG,[2] GEOFF WEST,[2] AND TINGYUN WANG[1]

[1]*Key Laboratory of Specialty Fiber Optics and Optical Access Networks, Joint International Research Laboratory of Specialty Fiber Optics and Advanced Communication, Shanghai Institute for Advanced Communication and Data Science, Shanghai University, 99 Shangda Road, Shanghai 200444, China*
[2]*WMG, University of Warwick, Coventry CV4 7AL, UK*
[*]*wenjx@shu.edu.cn*

Abstract: We have explored an orbital angular momentum (OAM) amplifier of 10 vortex modes under different-order OAM pump modes, i.e. OAM_0, OAM_1, and OAM_2. The all-fiber amplification system consists of an active few-mode erbium-doped fiber (FM-EDF), a mode selective pump (MSP), and a mode selective signal (MSS). These mode selective components are based on fused-taper mode selective couplers (MSC) under different wavelengths fabricated by a passive ring-core fiber (RCF). Under different-order mode pumps, the OAM amplifier experimentally exhibits mode gains (MGs) above 15 dB for 10 vortex modes with the mode purities only 89%, essentially in line with the simulation results. Especially when the signal-mode profiles are better matched to the pump-mode profiles, i.e. the OAM pumps with the same order as signals, the obtained MGs are all over 20.2 dB and the amplified OAM mode purity is up to 97%; the acquired noise figures (NFs) are <4.9 dB and even the minimum NF is 3.2 dB. The results reveal that the OAM amplifier shows low-NF and high-purity characteristics under configurable pump modes in C-band. The amplified high-order OAM mode could be promising for uses in the long-distance mode division multiplexing (MDM) and in mitigation of the upcoming capacity crunch in optical fiber communication.

1. Introduction

Optical fiber communication technology based on single mode fibers (SMFs) has been progressed rapidly during the last several decades, and data-carrying capacity of SMF has been approaching to its limit, facing the constraints to meet the increasing needs of big data (also referred to as capacity crunch) [1]. Nowadays, space division multiplexing (SDM) [2] is regarded as the critical technology for substantially improving the capacity of optical fiber communication. Within the various SDM approaches, mode division multiplexing (MDM) [3] that utilizes vortex beams has attracted increasing research interest. A vortex beam, also called an orbital angular momentum (OAM) beam, has a helical phase front. The phase can be expressed as $exp(il\theta)$, where l is the topological charge, and θ is the azimuthal angle around the optical axis, carrying an OAM of $l\hbar$ per photon [4,5]. Because of its unique characteristics, the OAM beam has been the subject of many advanced applications, such as optical tweezers [6], high-precision microscopy [7], atom manipulation [8], and information encoding and decoding [9]. Driven by these demands, a variety of free-space or fiber-based solutions for generating OAM beam have been proposed, including spatial light modulators [10], spiral phase plates [11], fiber gratings [12], and fiber couplers [13]. The optical fiber-based method has the low crosstalk between adjacent modes and can achieve stable transmission of data in long range [14,15], in which the signal intensity

#452410 https://doi.org/10.1364/OE.452410
Journal © 2022 Received 28 Dec 2021; revised 18 Feb 2022; accepted 20 Feb 2022; published 25 Feb 2022

Optics EXPRESS

could be maintained by amplifiers during optical communication. Up to now, it has been realized that the OAM mode amplifiers of first- [16], second- [17], third- [18], and fourth- [19] order OAM modes based on fundamental-mode pump with different multimode EDFs. In a multimode active fiber, mode gain (MG) relies on three factors, i.e. the concentration profile of the rare earth dopant ions, the pump intensity profile, and the signal intensity profile [20]. Therefore, high MG can be achieved by well-matching the signal mode profile and pump intensity profile, which means that utilizing a suitable pump mode to amplify a certain signal mode can experience high pump efficiency and even obtain low noise figure (NF) and high mode purity; However, these parameters, also important for the OAM amplifier, have not been investigated in previous papers. Moreover, the research on the high-order mode pump, or even high-order OAM mode pump, only stays at the theoretical stage and do not be proven experimentally.

In this paper, we investigate an OAM mode amplifier with the utilization of different-mode pumps, which is based on a home-made few-mode erbium-doped fiber (FM-EDF) and a ring-core fiber (RCF). By comparison with the different-mode pumps, the desirable performance of the OAM amplifier is implemented with low NF and high purity.

2. Fabrication and amplification properties of FM-EDF

Two kinds of silica optical fibers, namely the RCF and FM-EDF, are fabricated based on the modified chemical vapor deposition (MCVD) process. The fabrication of RCF consists of six steps: deposition of a loose body inside a substrate tube, incorporation of high-concentration doped materials (GeO_2), semi-vitrification, deposition of core layer with SiO_2, vitrification and shrinkage of the rod, and optical fiber drawing. FM-EDF is made using the liquid phase doping technique within the context of MCVD. The first step is to obtain porous core layers within a substrate tube followed by immersing the tube in a solution containing erbium ions. The second step is to drain out of the solution inside the tube and dehydrate it. Subsequently, the loose core layers containing erbium ions within the tube are fully sintered and the resultant tube with doped erbium ions is collapsed into a solid glass rod. Finally, the preform is drawn into an optical fiber.

Figure 1 (a) shows the typical refractive index distributions of RCF and FM-EDF. The RCF has a $D_{core} = 6.5$ μm, a $D_{ring} = 18.0$ μm, and a $D_{cladding} = 125.0$ μm. The structure renders a large refractive index difference up to 0.027. The refractive index profile also reveals a symmetrical bimodal structure with a central depletion due to the evaporation of germanium atoms during the fabrication process. The FM-EDF has a $D_{core} = 20.6$ μm and a $D_{cladding} = 125.0$ μm with the refractive index difference of 0.011 between the core and cladding layers. In addition, the excitation-emission spectra of the FM-EDF are shown in Fig. 1 (b), where the excitation and emission peaks are located at 979 nm and 1530 nm, respectively. The fluorescence lifetime of erbium ions on FM-EDF is 10.4 ms under 980 nm excitation. According to the fiber parameters, the effective mode refractive index (n_{eff}) of each mode in the RCF and FM-EDF are simulated, as shown in Figs. 1 (c) and (d) respectively. It should be noted that in theory the RCF and FM-EDF are able to support up to 18 and 14 vortex modes, i.e. $|l|=5$ and $|l|=3$, for data transmission respectively.

The mode patterns and phase distributions of different-order OAM modes in signal and pump are simulated in FM-EDF, as depicted in Fig. 2(a), whose normalized intensity profiles and erbium-doped profile are shown in Fig. 2(b). Since the intensity profiles and n_{eff} of degenerate modes in each order OAM are almost identical; accordingly for simplicity, only one mode of each order OAM is taken into consideration. MG mainly depends on the concentration profile of the rare earth dopant ions, the pump intensity profile, and the signal intensity profile. In general, a signal mode whose profile is better matched to the pump intensity profile will obtain higher gain. Hence, by controlling the pump mode, it can be realized the configurable MG. The numerical simulation of different mode amplification in the FM-EDF has been carried out by the rate and

Optics EXPRESS

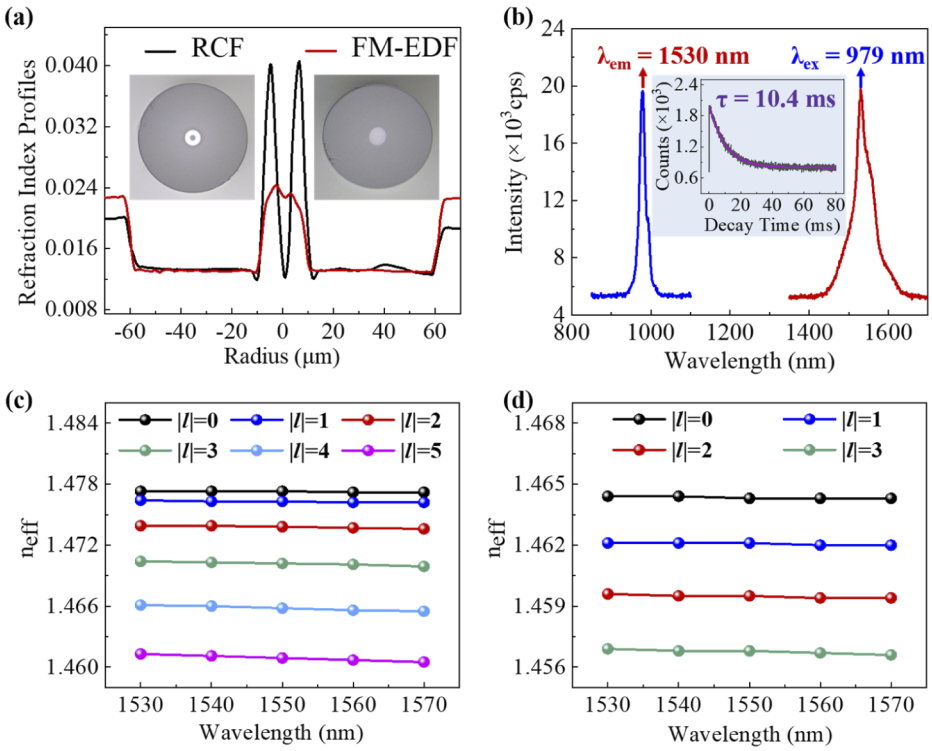

Fig. 1. (a) Refractive index profiles and cross-sectional views (inset) of RCF and FM-EDF. (b) Excitation-emission spectra of FM-EDF, where the inset is fluorescence decay curve of the FM-EDF. Simulated n_{eff} as a function of the wavelength from 1530 to 1570 nm in (c) RCF, and (d) FM-EDF.

power propagation equations, which can be expressed as (1)-(4) [21].

$$\frac{dP_{s,m}(z)}{dz} = P_{s,m}(z)\int_0^{2\pi}\int_0^{a}[\sigma_{es}N_2(r,\varphi,z) - \sigma_{as}N_1(r,\varphi,z)]\Gamma_{s,m}(r,\varphi)rdrd\varphi, \tag{1}$$

$$\frac{dP_{p,n}(z)}{dz} = -P_{p,n}(z)\int_0^{2\pi}\int_0^{a}\sigma_{ap}N_1(r,\varphi,z)\Gamma_{p,n}(r,\varphi)rdrd\varphi, \tag{2}$$

$$N_2(r,\varphi,z) = \frac{\left[\frac{1}{h\nu_p}P_{p,n}(z)\sigma_{ap}\Gamma_{p,n}(r,\varphi) + \frac{1}{h\nu_s}\sum_m P_{s,m}(z)\sigma_{as}\Gamma_{s,m}(r,\varphi)\right]N_0(r,\varphi,z)}{\frac{1}{h\nu_p}P_{p,n}(z)\sigma_{ap}\Gamma_{p,n}(r,\varphi) + \frac{1}{h\nu_s}\sum_m P_{s,m}(z)(\sigma_{es}+\sigma_{as})\Gamma_{s,m}(r,\varphi) + \frac{1}{\tau}}, \tag{3}$$

$$N_1(r,\varphi,z) = N_0(r,\varphi,z) - N_2(r,\varphi,z), \tag{4}$$

where $P_{s,m}$ and $P_{p,n}$ are the m-th signal mode power and n-th pump power, $\Gamma_{s,m}$ and $\Gamma_{p,n}$ are the power overlap integrals of signal light and pump light that are related to the optical intensity distribution of signal or pump light, N_1, N_2 and N_0 are the lower energy level, upper energy level and total doping concentration of erbium ions in the FM-EDF respectively, σ_{as}, σ_{es} and σ_{ap} are the absorption and emission cross-sectional area of signal light and the absorption cross-sectional area of pump light respectively, and ν_s and ν_p are the optical frequencies of signal and pump

Optics EXPRESS

lights. The last two optical frequencies are related to their respective wavelengths λ_s and λ_p, and can be expressed as $\nu = c / \lambda$ where c is the speed of light, h is the Planck constant, and τ is the erbium ions lifetime in the FM-EDF. The model is solved using the method of the 4th-order Runge-Kutta calculation [22].

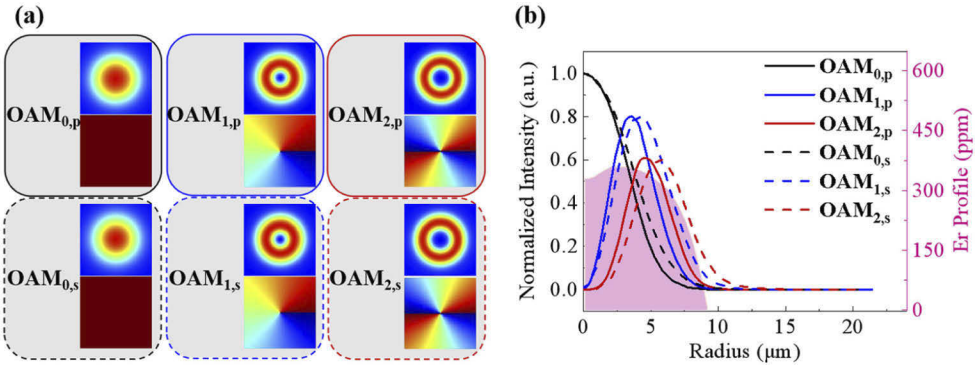

Fig. 2. (a) Simulated OAM mode patterns and phase distributions and (b) normalized intensity profiles of OAM_0, OAM_1, and OAM_2 in signal and pump mode and erbium-doped profile of FM-EDF.

Figures 3 (a)-(c) show the MGs against the fiber length, where the gain reaches its saturation at the ~1.4 m. As such, this theoretical optimal fiber length is utilized to work out the MGs of 10 vortex modes as the function of wavelength under OAM_0, OAM_1 and OAM_2 pump, as shown in Figs. 3 (d)-(f). It has been found that the MGs are higher than 15 dB and essentially remain within a range across the wavelengths of 1530-1550 nm. For the OAM pump with the same-order as the signal, the MGs are relatively higher, possibly resulting from the larger overlap integrals of the same-order OAM pump and signal in FM-EDF, which is better to maintain the signal profiles for transmission.

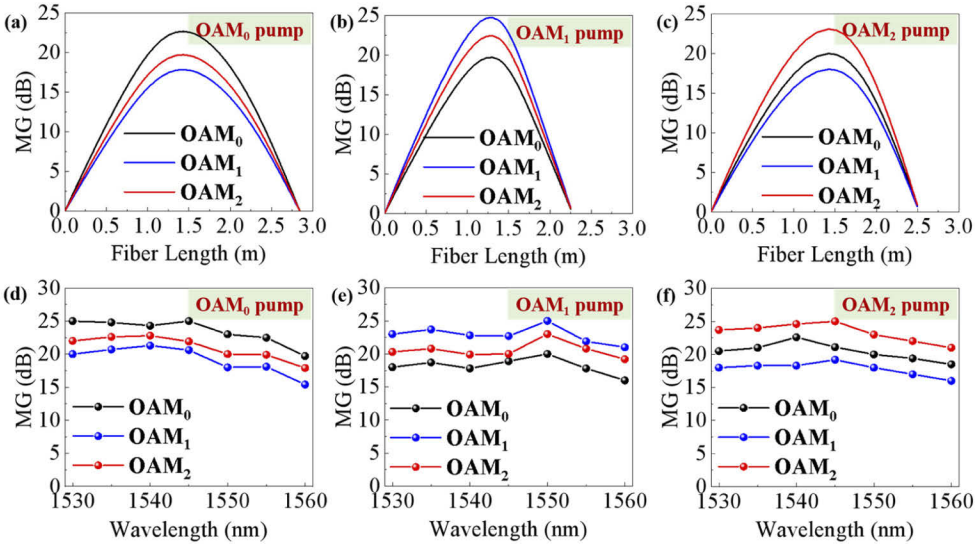

Fig. 3. Simulated MGs as a function of (a)-(c) fiber length and (d)-(f) wavelength of FM-EDF under 980 nm OAM_0 pump, OAM_1 pump, and OAM_2 pump respectively.

Optics EXPRESS

3. Generation of OAM pump and signal modes

According to the fiber parameters of a standard SMF and the home-made RCF, a fused taper mode selective coupler (MSC) is fabricated to generate OAM modes based on the coupled mode theory [23]. To realize the mode coupling, two modes need to satisfy the phase-matching condition, i.e., they need to have the same value of n_{eff} [13]. As such, the relationship between n_{eff} and the RCF ring radius at 980 and 1550 nm are investigated, as shown in Figs. 4 (a) and (b), respectively. Under 980 nm, when the LP_{01} mode in SMF and LP_{11} and LP_{21} modes in RCF have the same value of n_{eff}, scaling factor $\rho = R_{SMF} / R_{RCF} = 0.7$ and 0.49, indicating that the SMF should have the cladding diameter of 87.5 and 61.3 μm after pre-stretched. Experimentally, the SMF is made with a cladding diameter of 90.4 and 65.1 μm to generate LP_{11} and LP_{21} mode, closely matching the calculated value. Also under 1550 nm, the generation of LP_{11} and LP_{21} modes is based on the pre-stretched SMF with a cladding diameter of 109.8 and 86.5 μm. Upon the simulation results, the mode conversion coupler has been fabricated using the fused taper technology (manufacturing details in Ref. [16]). Figure 4 (c) shows the transverse mode fields of OAM_1 and OAM_2 modes and their interferogram of the MSCs output at 980 nm and ~1550 nm.

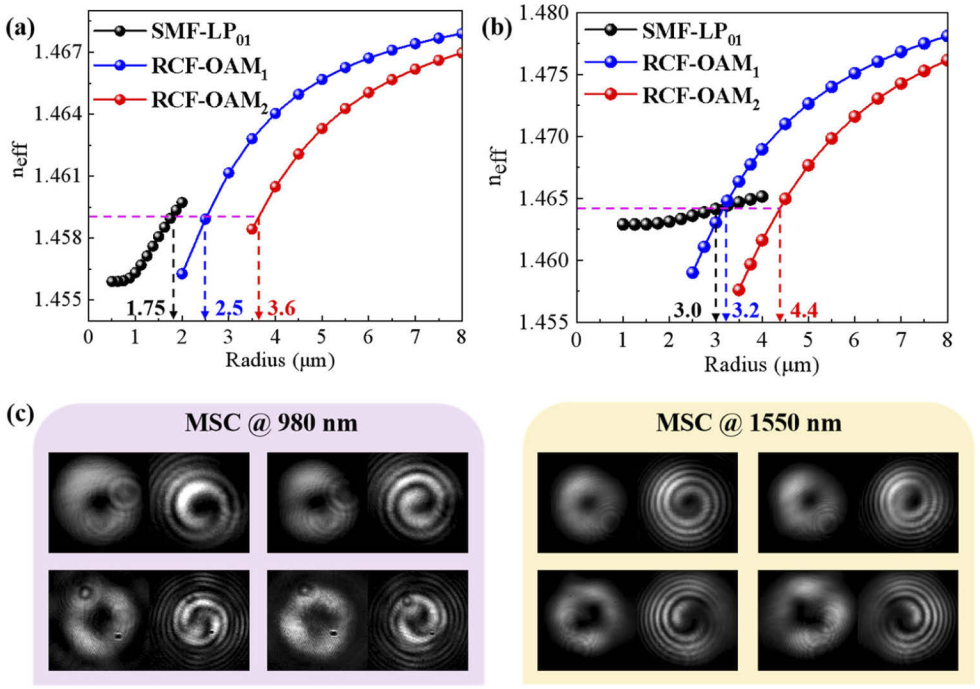

Fig. 4. n_{eff} of LP_{01} mode in the SMF and high-order OAM modes in the RCF as a function of core and ring radius at (a) 980 nm and (b) 1550 nm, respectively. (c) The transverse mode fields of OAM_1 and OAM_2 modes and their interferogram of the MSCs output at 980 nm and 1550 nm.

4. Amplification and feature analysis of OAM modes

An all-fiber OAM mode amplification system is built up, as shown in Fig. 5. It consists of three main sections, i.e., mode selective pump (MSP), mode selective signal (MSS), and FM-EDF. A 980 nm laser supplies sufficient pump power and is connected to a MSC1 to generate high-order modes. The state of polarization (SOP) of the output light is regulated by a polarization controller 1 (PC1) for the OAM-mode pump generation. A tunable laser source (TLS, Santec TSL-710) is

Optics EXPRESS

used to provide fundamental mode beam at different wavelengths from 1530 to 1560 nm, which can be coupled and converted to high-order modes in the MSC2. Similarly, PC2 is used for tuning SOP to generate the OAM-mode signal. A 3:7 coupler can divide the beam into two channels in a fixed proportion: one is the interference beam and the other is the signal light. Few-mode wavelength division multiplexer (FM-WDM) combines the OAM pump and signal into the FM-EDF with the 1.4 m length. FM-WDM fabricated with the homemade RCF can maintain the OAM mode transmission. Band-pass optical filter (BF, Thorlabs FB1550-12, FWHM = 12 nm) is employed to filter out the narrow-band beam and reduce the amplified spontaneous emission (ASE) effect. The character 'M' refers to a reflection mirror. The vortex beam and the fundamental mode beam is combined by a beam combiner (BC), a neutral attenuator (NA) can balance the power of beam in both channels, and a charge coupled device (CCD, HAMAMATSU C10633) camera is employed for real-time observation of the intensity distribution of transverse mode field. An optical spectrum analyzer (OSA, Yokogawa AQ-6370D) is used to record the amplified spectra. The experimentally observed transverse mode fields and the corresponding interferogram with different pump modes are shown in Fig. 6 (a). Note that the interferogram of zero, one, and two spiral stripes are obtained, indicating that OAM_0, OAM_1, and OAM_2 mode can transmit along the FM-EDF with different-order OAM pump modes.

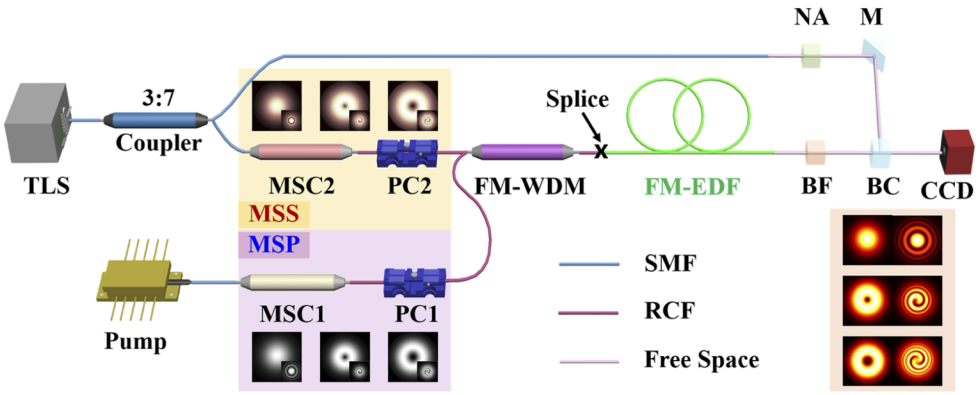

Fig. 5. Schematic diagram of an all-fiber broadband OAM mode amplification and detection system. TLS, tunable laser source; MSC, mode selective coupler; MSP, mode selective pump; MSS, mode selective signal; PC, polarization controller; FM-WDM, few-mode wavelength division multiplexer; FM-EDF, few-mode erbium-doped fiber; BF, band-pass filter ; BC, beam combiner; NA, neutral attenuator; M, reflection mirror; CCD, charge coupled device; OSA, optical spectrum analyzer.

The purity of OAM modes after amplification at 1550 nm is evaluated under OAM_0, OAM_1, and OAM_2 pump using the method of ring technique [4,13]. The measurement results are illustrated in Fig. 6 (b). One can see that the OAM mode purities are only above 89%. However, when the signal modes are consistent with the pump modes, the OAM mode purities obtained are higher, which may be due to the higher pump efficiency when the OAM pump modes have the same topological charge as the OAM signal modes, especially the purity of OAM_1 mode launched by the OAM_1 pump up to 97%, illustrating high mode purity of the OAM amplifier. Additionally, it is not introduced other high-order signal modes in the OAM_0 mode amplification. Therefore, it can be said that the high-purity amplification of 10 vortex modes is achieved. This high-purity OAM mode amplification is of great significance to the MDM systems.

In order to evaluate the amplifier performance, the spectra before and after the amplification are measured for the signal and pump modes of OAM_0, OAM_1, and OAM_2. A signal power of -20 dBm is constantly used throughout the experiment. Figures 7 (a)-(c) shows the MGs and

Optics EXPRESS

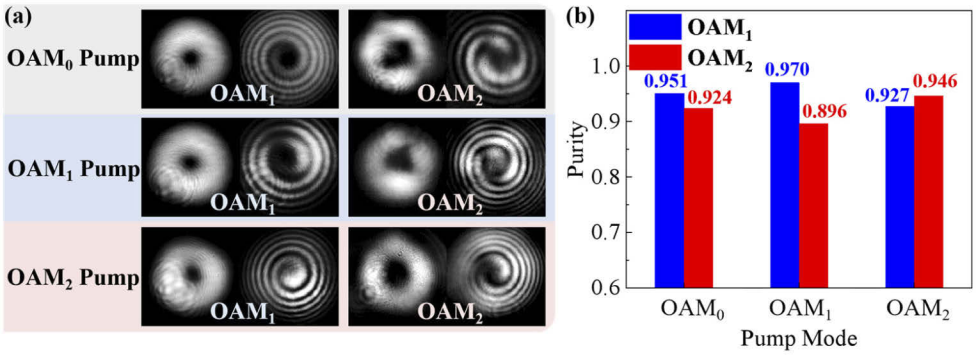

Fig. 6. (a) The amplified OAM_0, OAM_1, and OAM_2 modes and their interferograms, and (b) the mode purity measured at 1550 nm under OAM_0, OAM_1, and OAM_2 pump.

NFs across 1530-1560 nm signal wavelengths under OAM_0, OAM_1, and OAM_2 pump with the constant pump power of 700 mW. NF can be calculated by the equation as (5) [24].

$$NF\ (dB) = 10\log\left(\frac{1}{G} + \frac{p_{ASE}}{Gh\nu B_0}\right), \tag{5}$$

where G represents the MG of each mode under the central wavelength of $\lambda = c\ /\ \nu$. P_{ASE} represents the ASE power (average value of the power separated by 0.3 nm on both sides of λ). B_0 is the effective bandwidth expressed by $c{\cdot}\Delta\lambda\ /\ \lambda^2$, where $\Delta\lambda$ is the resolution of the OSA, which is 0.02 nm in this case. Note that MGs are above 15 dB and can maintain the fluctuation value less than 3.5 dB, which is consistent with the simulation results. Also note that when signals and pumps with the same-order OAM modes, MGs are larger than the other two pump modes, i.e. above 20.2 dB, and NFs are less than 4.9 dB for all 10 vortex modes under the pumps with the power of 700 mW, even the minimum NF is 3.2 dB. It may be due to the larger overlap integral of OAM pump and signal light with the same order in FM-EDF, which may contribute to

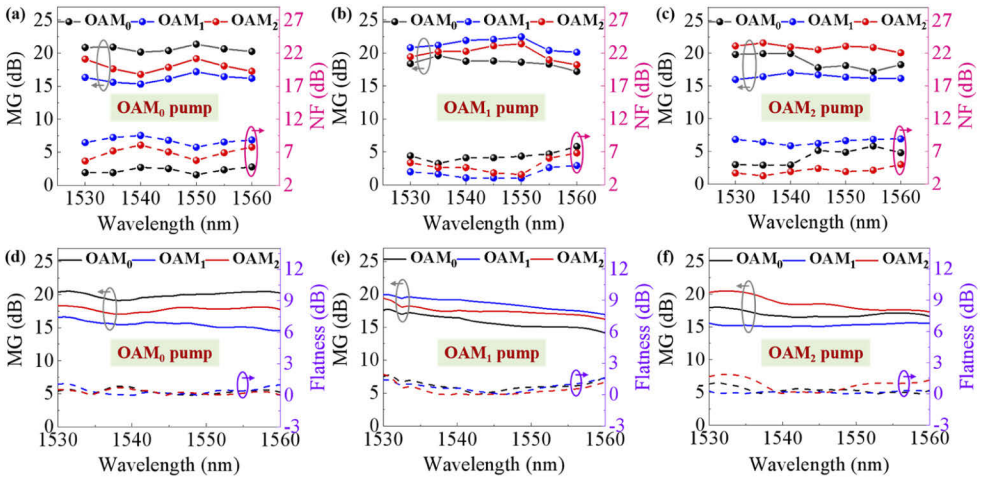

Fig. 7. The gain characteristics of the amplification system. MGs and NFs as a function of wavelength under the (a) OAM_0, (b) OAM_1, and (c) OAM_2 pump power of 700 mW. MGs and gain flatness measured with the broad spectrum under the (d) OAM_0, (e) OAM_1, and (f) OAM_2 pump power of 700 mW.

Optics EXPRESS

the improvement of the mode purity in the amplifier. One can see that the MGs in the experiment are relatively smaller than those in the simulation. It might be due to the ASE effect occurred in the experiment as previously discussed, which is not taken into account in the simulation.

Furthermore, a broadband light source is connected to the system for the signal light, instead of the TLS (Fig. 5) to assess the broad-spectrum characteristic of the OAM amplifier. The signal-light spectrum spans from 1530 to 1560 nm with the power of ~-20 dBm. The comparable broad-spectrum MGs and the flatness have accomplished in the range of 1530-1560 nm under the different-order pump with the power of 700 mW, as shown in Figs. 7 (d)-(f). Note that the broad-spectrum MGs are above 15 dB for all 10 vortex modes, which present the same tendency as single-wavelength amplification, i.e. the larger MGs are obtained when signals and pumps with the same-order OAM modes. Also note that the gain fluctuations are all less than 1.9 dB, implying the great gain flatness. In general, the broad-spectrum MGs are relatively lower than the single-wavelength ones, maybe because MGs will be affected by the ASE generated in all wavelengths in broadband amplification, resulting in the larger noise and lower gain for the amplifier.

5. Conclusions

In conclusion, we have demonstrated an OAM amplifier for 10-vortex-mode amplification under configurable pump modes using purposely fabricated two kinds of fibers, RCF and FM-EDF. Through the theoretical analysis and simulation, the MGs of OAM_0, OAM_1, and OAM_2 in the FM-EDF generally maintain in the range of 1530-1560 nm under different mode pumps. In the experiment, we first fabricate two MSCs by the home-made passive RCF together with a SMF, through which the conversion of fundamental mode to the OAM_1 and OAM_2 mode are accomplished at the wavelengths of 980 nm and ~1550 nm, implying that the MSCs can be employed for a MSP and a MSS respectively. Subsequently, the generated OAM modes are amplified using the active FM-EDF, on which an all-fiber OAM amplification system is constructed. In this amplification system, the OAM amplifier presents MGs above 15 dB for 10 vortex modes under different-order mode pumps. In particular, when the signal-mode profiles are better matched to the pump-mode profiles, i.e. the OAM pumps with the same order as signals, the MGs are above 20.2 dB with the OAM mode purity up to 97%, and NFs are less than 4.9 dB with a minimum of 3.2 dB. The results show that our OAM amplifier can realize low NF and high purity under configurable pump modes in C-band. Additionally, the broad-spectrum amplification is discussed, in which the gain fluctuations are all less than 1.9 dB from 1530 to 1560 nm. The all-fiber OAM amplification in this work has a potential application in the long-distance optical fiber communication, such as high-order optical vortex amplifiers, lasers, light sources, and so on. Next, we will further optimize the parameters of RCF and FM-EDF to obtain better mode matching, and will further investigate the amplifiers of higher MG and more modes with lower NF.

Funding. National Key Research and Development Program of China (2018YFB1801800, 2020YFB1805800); National Natural Science Foundation of China (61935002, 61975113); Shanghai professional technical public service platform of advanced optical waveguide intelligent manufacturing and testing (19DZ2294000); 111 Project (D20031).

Acknowledgements. This work was supported by National Key Research and Development Program of China (Grant Nos. 2018YFB1801800, 2020YFB1805800) and National Natural Science Foundation of China (Grant Nos. 61975113, 61935002); Shanghai professional technical public service platform of advanced optical waveguide intelligent manufacturing and testing (19DZ2294000); 111 Project (D20031).

Disclosures. The authors declare no conflicts of interest.

Data availability. Data underlying the results presented in this paper are not publicly available at this time but may be obtained from the authors upon reasonable request.

Optics EXPRESS

References

1. R. J. Essiambre, G. Kramer, P. J. Winzer, G. J. Foschini, and B. Goebel, "Capacity limits of optical fiber networks," J. Lightwave Technol. **28**(4), 662–701 (2010).
2. D. J. Richardson, J. M. Fini, and L. E. Nelson, "Space-division multiplexing in optical fibres," Nat. Photonics **7**(5), 354–362 (2013).
3. N. Bozinovic, Y. Yue, Y. X. Ren, M. Tur, P. Kristensen, H. Huang, A. E. Willner, and S. Ramachandran, "Terabit-scale orbital angular momentum mode division multiplexing in fibers," Science **340**(6140), 1545–1548 (2013).
4. S. Ramachandran and P. Kristensen, "Optical vortices in fiber," Nanophotonics **2**(5-6), 455–474 (2013).
5. N. Bozinovic, S. Golowich, P. Kristensen, and S. Ramachandran, "Control of orbital angular momentum of light with optical fibers," Opt. Lett. **37**(13), 2451–2453 (2012).
6. M. Padgett and R. Bowman, "Tweezers with a twist," Nat. Photonics **5**(6), 343–348 (2011).
7. O. J. Allegre, W. Perrie, S. P. Edwardson, G. Dearden, and K. G. Watkins, "Laser microprocessing of steel with radially and azimuthally polarized femtosecond vortex pulses," J. Opt. **14**(8), 085601 (2012).
8. H. Kawauchi, K. Yonezawa, Y. Kozawa, and S. Sato, "Calculation of optical trapping forces on a dielectric sphere in the ray optics regime produced by a radially polarized laser beam," Opt. Lett. **32**(13), 1839–1841 (2007).
9. L. C. Crasovan, G. Molina-Terriza, J. P. Torres, L. Torner, V. M. Pérez-García, and D. Mihalache, "Globally linked vortex clusters in trapped wave fields," Phys. Rev. E **66**(3), 036612 (2002).
10. A. Cofré, P. García-Martínez, A. Vargas, and I. Moreno, "Vortex beam generation and other advanced optics experiments reproduced with a twisted-nematic liquid-crystal display with limited phase modulation," Eur. J. Phys. **38**(1), 014005 (2017).
11. M. W. Beijersbergen, R. P. C. Coerwinkel, M. Kristensen, and J. P. Woerdman, "Helical-wavefront laser beams produced with a spiral phaseplate," Opt. Commun. **112**(5-6), 321–327 (1994).
12. Y. Zhao, Y. Liu, L. Zhang, C. Zhang, J. Wen, and T. Wang, "Mode converter based on the long-period fiber gratings written in the two-mode fiber," Opt. Express **24**(6), 6186–6195 (2016).
13. S. Pidishety, S. Pachava, P. Gregg, S. Ramachandran, G. Brambilla, and B. Srinivasan, "Orbital angular momentum beam excitation using an all-fiber weakly fused mode selective coupler," Opt. Lett. **42**(21), 4347–4350 (2017).
14. N. Bozinovic, P. Kristensen, and S. Ramachandran, "Long-range fiber-transmission of photons with orbital angular momentum," in *Conference on Lasers and Electro-Optics*, 2011 OSA Technical Digest Series (Optical Society of America, 2011), Paper CTuB1.
15. P. Gregg, P. Kristensen, and S. Ramachandran, "Conservation of orbital angular momentum in air-core optical fibers," Optica **2**(3), 267–270 (2015).
16. J. Wen, X. He, J. Xing, J. Yang, F. Pang, X. Zeng, Z. Chen, and T. Wang, "All-fiber OAM amplifier with high purity and broadband spectrum gain based on fused taper vortex-beam coupler," IEEE Photonics J. **10**(6), 1 (2018).
17. Y. Wu, X. He, J. Wen, F. Pang, Z. Chen, X. Zeng, and T. Wang, "All-fiber second-order OAM amplifier based on mode selective coupler," in *Conference on Lasers and Electro-Optics*, 2020 OSA Technical Digest Series (Optical Society of America, 2020), Paper STu3R.3.
18. X. Zhang, J. Liu, S. Chen, W. Li, C. Du, and J. Wang, "Amplification of 14 orbital angular momentum modes in ring-core erbium-doped fiber with high modal gain," Opt. Lett. **46**(22), 5647–5650 (2021).
19. T. Wen, S. Gao, W. Li, J. Tu, C. Du, J. Zhou, Z. Ao, B. Zhang, W. Liu, and Z. Li, "Third- and fourth-order orbital angular momentum multiplexed amplification with ultra-low differential mode gain," Opt. Lett. **46**(21), 5473–5476 (2021).
20. N. Bai, E. Ip, T. Wang, and G. Li, "Multimode fiber amplifier with tunable modal gain using a reconfigurable multimode pump," Opt. Express **19**(17), 16601–16611 (2011).
21. M. Gong, Y. Yuan, C. Li, P. Yan, H. Zhang, and S. Liao, "Numerical modeling of transverse mode competition in strongly pumped multimode fiber lasers and amplifiers," Opt. Express **15**(6), 3236–3246 (2007).
22. Q. Kang, E. L. Lim, Y. Jung, J. K. Sahu, F. Poletti, C. Baskiotis, S. Alam, and D. J. Richardson, "Accurate modal gain control in a multimode erbium doped fiber amplifier incorporating ring doping and a simple LP01 pump configuration," Opt. Express **20**(19), 20835–20843 (2012).
23. W. Huang, "Coupled-mode theory for optical waveguides: An overview," J. Opt. Soc. Am. A **11**(3), 963–983 (1994).
24. K. S. Abedin, T. F. Taunay, M. Fishteyn, M. F. Yan, B. Zhu, J. M. Fini, E. M. Monberg, F. V. Dimarcello, and P. W. Wisk, "Amplification and noise properties of an erbium-doped multicore fiber amplifier," Opt. Express **19**(17), 16715–16721 (2011).